

A STUDY OF A DEVELOPING WAVE CYCLONE

T. N. KRISHNAMURTI

Department of Meteorology, Florida State University, Tallahassee, Fla.

ABSTRACT

In the past most diagnostic studies of frontal cyclone development have been carried out through use of quasi-geostrophic models. In this paper we present the results of vertical motions obtained from a 5-level general balance model. Nongeostrophic effects such as deformation and beta term of the balance equations, divergence, vertical advection, and the twisting term of the complete vorticity equation are retained. Advection of thermal and vorticity fields by the divergent part of the wind are also included in this analysis. Diabatic effect through release of latent heat in regions of saturated dynamic ascent, frictional effects at the lower boundary, and sensible heat transfer from the lake waters to the atmosphere are additional features. The results are presented in a partitioned form. The main results of the calculation reveal that: in the initial diffluent stage of the upper trough pronounced sinking motions behind the trough are associated with a strong field of convergence in the northwesterly flow in the upper trough. This sinking motion is partitioned to arise primarily from differential vorticity advection by nondivergent part of the wind, Laplacian of thermal advection by nondivergent part of the wind, and the terrain downslope motion. The upper level development is followed by intense surface cyclogenesis during a period of approximately 36 hr. During the latter stages development is found to be associated with intense rising motion arising from differential vorticity advection by the nondivergent part of the wind, Laplacian of thermal advection by the nondivergent part of the wind, latent heat, and surface friction.

1. INTRODUCTION

The case study deals with the application of a diagnostic balance model [3] to a frontal cyclone development over the midwestern United States. This is an extension of a study of the same storm reported by Krishnamurti, Nogues, and Baumhefner [4]. The important difference in the two models is the inclusion here of the effects of terrain, friction, latent and sensible heat. Some minor revisions in the scaling of dynamical equations are also incorporated in this version.

Analysis of the following fields were carried out for Apr. 12 and 13, 1964:

- i) Geopotential heights of standard constant pressure surfaces
- ii) Specific humidity at standard constant pressure surfaces
- iii) Cloud cover using conventional and TIROS data.

The following calculations were carried out for four map times of storm development:

- i) Three dimensional motion field using a two level quasi-geostrophic model (adiabatic)
- ii) Three dimensional motion field using a 5-level linear balance model (adiabatic)
- iii) Three dimensional motion field using a 5-level general balance model, including effects of terrain, friction, and heating
- iv) Partitioning of vertical motion for the various models
- v) Three dimensional trajectories and interpolation of development terms along the trajectory.

Since approximately 10^4 two dimensional fields are computed and stored as binary records on magnetic tapes, it becomes quite a difficult task to isolate important features and portray them for illustration purposes. Not all map times showing the development of any feature is shown in the following. A selection of some of the important features are made, but it is quite possible that

some important information has thus been omitted in the following discussions.

2. SYNOPTIC SITUATION DURING WAVE CYCLONE DEVELOPMENT

The case study was selected because of a development that followed the well known criteria of the two level quasi-geostrophic theory. In the upper levels there was a well marked diffluent through initially (fig. 1, Apr. 12, 1964 00 GMT) with strong northwesterly flow in the rear of the upper trough, and weaker winds ahead of it. From simple barotropic considerations such a diffluent trough is expected to produce a stronger curvature and a drop in the 500-mb. height field due to a transformation of shear vorticity into curvature vorticity. In this case considerable development of the 500-mb. height field was noticed with an increase in the magnitudes of the absolute vorticity due to baroclinic processes. At the surface levels (fig. 2), there was a considerable development of a weak lee trough into a 975-mb. Low over Minnesota. We are depicting four map times at intervals of 12 hr., these may be approximately labeled to indicate the, i) diffluent stage, ii) open wave stage, iii) preocclusion stage, and iv) occlusion stage.

The trough, initially over the lee of the Rockies, moved a distance of about 1,000 n.mi. over a period of 36 hr. Since the major development took place in a region well covered with data it is possible to obtain detailed three dimensional analysis of the geopotential height distributions. The surface Low developed somewhat slowly in the first 24 hr. and a rapid development followed in the last 12 hr.

Figure 3 shows the geopotential heights and the isotachs of the total wind for the four map times at the 200-mb. surface. Unlike in the Tropics the upper level maps near the jet stream level in middle latitudes give limited qualitative information. There was a strong polar jet stream behind the upper trough at the first map time,

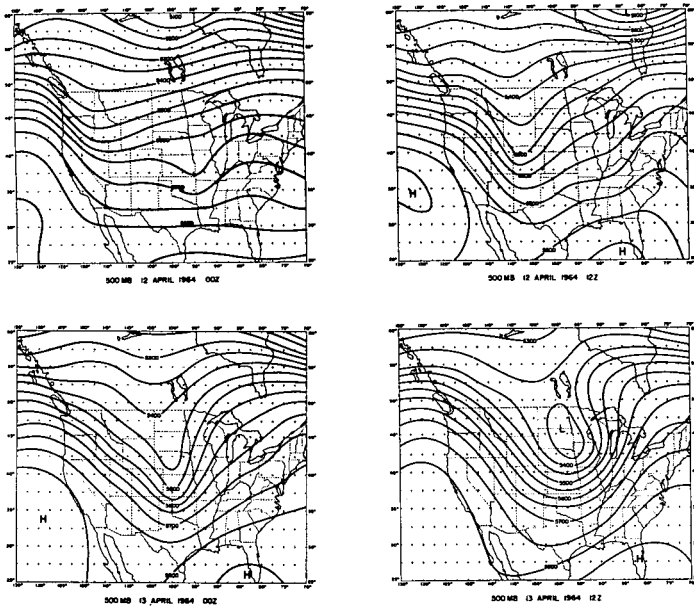


FIGURE 1.—500-mb. surface heights (meters) for four map times, April 12, 13, 1964.

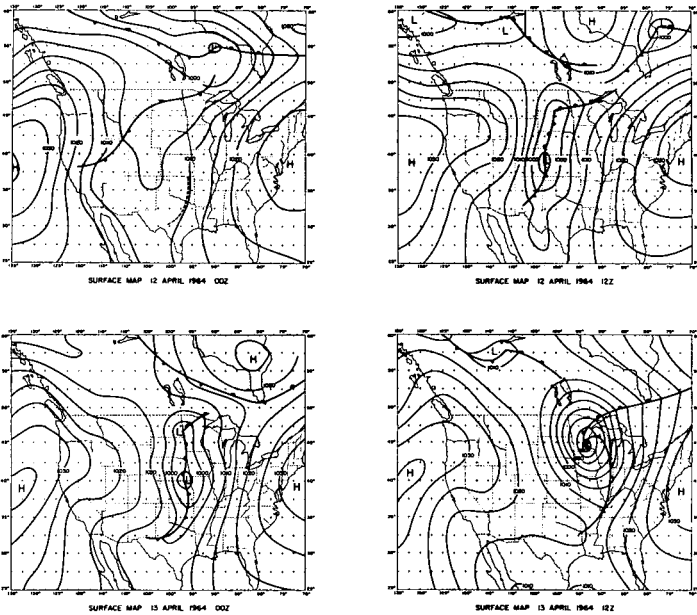


FIGURE 2.—Surface isobars for four map times, April 12, 13, 1964.

the jet stream moved faster than the wave, and a large part of the strong winds were equally well distributed on both sides of the upper trough by the last map time. The 500-mb. surface shows a more distinct change from a diffluent to a confluent system, a feature very typical during rapid cyclogenesis. Maps of specific humidity show a moist tongue well north to 40°N. extending from the Gulf of Mexico during all map times.

Figure 4 shows the distribution of total precipitable water for the four map times. This distribution was obtained from the fields of specific humidity at several levels using Simpson's rule of numerical integration in the vertical. This integrated map is not directly used in any of the subsequent calculations, but, the fields of specific humidity are used in the determination of heating terms. The integrated map is useful for discussion purposes. It shows a quasi-stationary moist tongue which may have

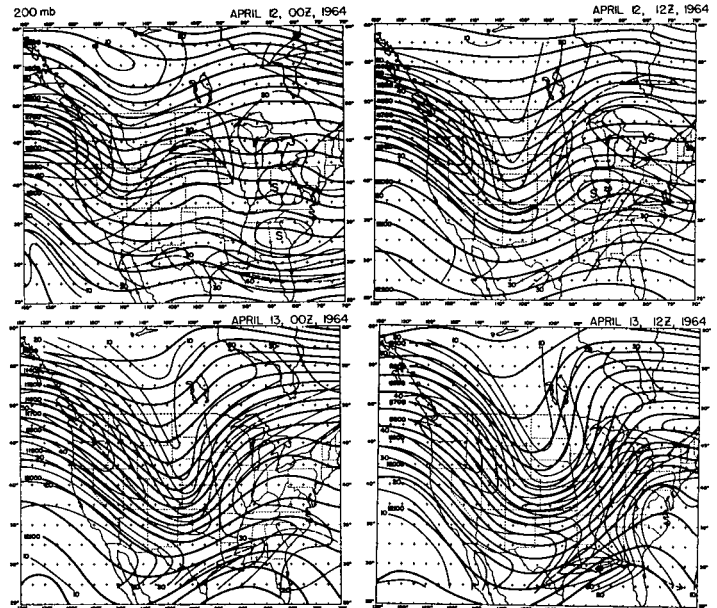


FIGURE 3.—200-mb. heights (meters) for four map times (heavy lines) and isotachs of the total wind (thin lines) m./sec.

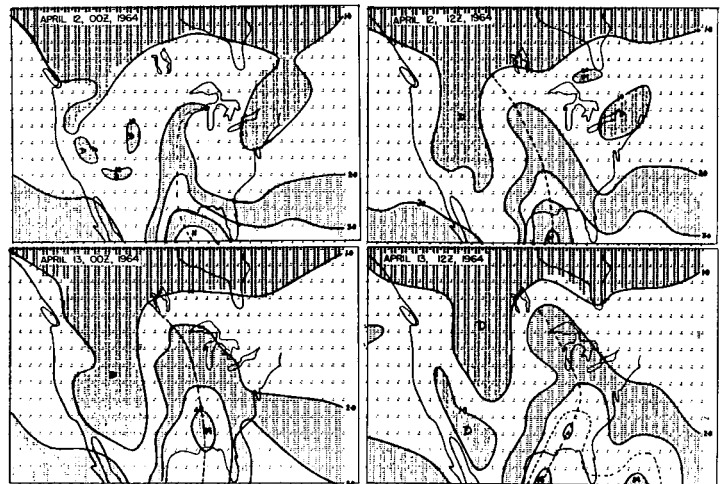


FIGURE 4.—Analysis of total precipitable water (cm.) for four map times.

played an important role in the development through precipitation, latent heat release, attendant rising motions, and low level convergence distributions. These are some of the questions that we hope to examine in the next sections. Precipitation amounts were small prior to April 13, 00 GMT. In the next 12 hr. several stations reported 1 to 2 in. of rain along the northern part of the moist tongue. We overlooked this precipitation when we first examined the regular surface synoptic reports. A reexamination of the hourly precipitation data over a large number of hourly recording stations in Minnesota showed that precipitation was indeed high in the last 12 hr.

Figure 5 illustrates nephanalysis for the four map times. Conventional data (synoptic reports for four map times) as well as satellite information (pictures and radiation measurements from channels II and V for ORBITS 4398, 4399, 4412, 4427, 4428, 4413 (only radiation), and 4414 (only pictures) of TIROS VII have been used. See

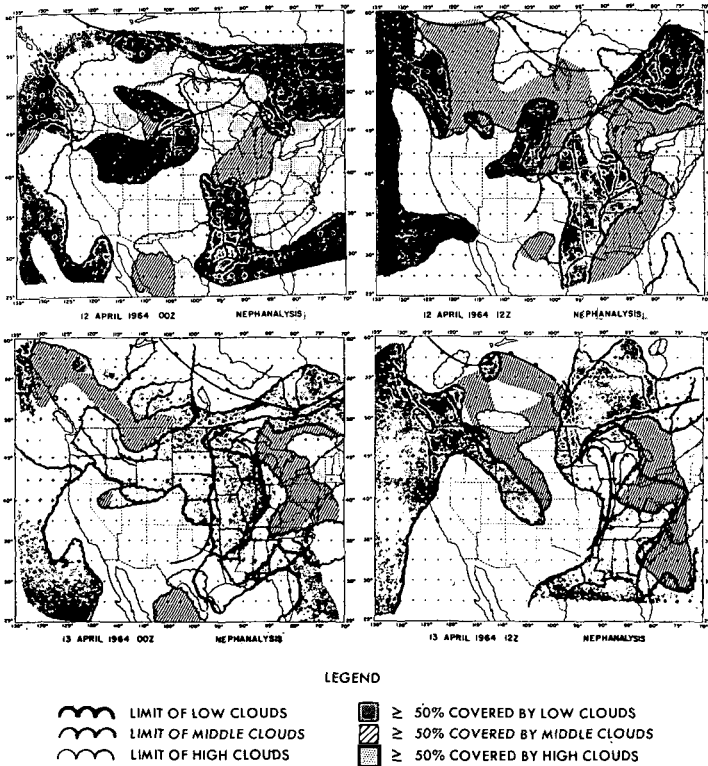


FIGURE 5.—Nephanalysis for April 12, 13, 1964, for four map times based on conventional and TIROS data.

figure 5. The conventional data have been mostly taken into account but wherever satellite information was available it was taken to support or complete the analysis.

The type of clouds and their amount have been considered. From nephanalysis we find that low cloudiness is found in the northwestern part of the Country, Pacific, and parts of the frontal system.

Wherever a zone with two types of cloudiness is found, shaded regions determine the dominant type and a line is drawn enclosing the region of both types. Thus in eastern Canada and Minnesota there is a dominating zone of stratus, stratocumulus and fractostratus that prevents seeing higher clouds. This is also confirmed by satellite information; therefore the line for middle clouds is included. There is a good correlation between region of heavy overcast with the fields of total precipitable water (fig. 4). At the first map time there was a region of overcast extending from the Gulf of Mexico northward to 40° lat. The organization of the pattern of cloud cover during the occlusion stage from an initial chaotic state is an interesting feature of this figure. Cloud patterns are generally interesting to look at when they are part of a vigorous isolated weather system; if there are several weak systems, patterns tend to be chaotic. This is generally true of any synoptic feature of atmospheric dynamics. Detailed synoptic studies of many interacting systems, in a domain of interest, usually leaves a number of unanswered questions.

Figure 6 illustrates the distribution for four map times of the vertical motions at the 500-mb. surface obtained from a multilevel linear balance model. *The unit of vertical velocity throughout this report is 10⁻⁵ mb./sec.* This

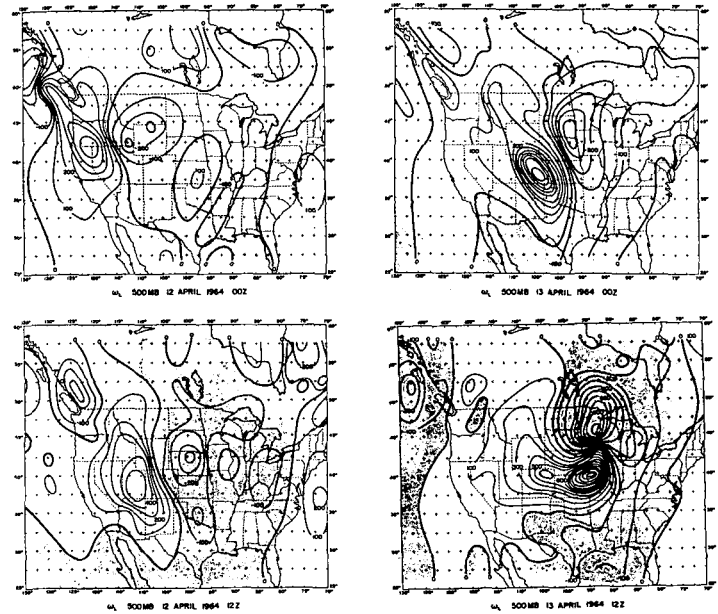


FIGURE 6.—Vertical velocity (10⁻⁵ mb./sec.) for April 12, 13, 1964. (Four map times.) The results apply at the 500-mb. surface. Calculations were made using a multilevel linear balance model.

corresponds to approximately 0.013 cm./sec. Of interest in the vertical motion distributions are the large sinking motions behind the diffluent trough at the first map time. The maximum sinking intensity is close to 500 units, maximum intensity of rising motions is only 200 units. The gradual increase in the intensity of the rising and sinking motions in the developing storm is worthy of note. The pattern of rising and sinking motions at the last map time is a classic illustration of the dipole centers during the occlusion stage.

3. A COMPARISON OF THE GEOSTROPHIC VS. THE BALANCED NONDIVERGENT WIND FIELDS

The balance equation for the nondivergent stream function is given by the equation,

$$\nabla \cdot f \nabla \psi = \nabla^2 \phi - 2J \left(\frac{\partial \psi}{\partial x}, \frac{\partial \psi}{\partial y} \right).$$

There are several approximations of interest here. i) If the second term on the right hand side is dropped and f is replaced by f_0 , a mean value of the Coriolis parameter, then the stream function ψ described geostrophic motions (Phillips [9]). ii) If f is treated as a variable and the second term is not retained then ψ_L describes what is frequently called a linear balanced nondivergent stream function. iii) If the geostrophic stream function is used to evaluate the second term on the right hand side and f is treated as a variable then ψ_{N1} is called a semigeostrophic balance stream function. iv) If no approximations are made then ψ_{N2} is called the complete nondivergent balanced stream function. This balance equation has been analyzed by several meteorologists over the past 10 yr. Petterssen [7] found this form of the equation in 1936 in his studies of the kinematic properties of the wind fields.

It is of interest to a synoptic meteorologist to find out if large motions can still be nondivergent. In 1951 Bjerknes

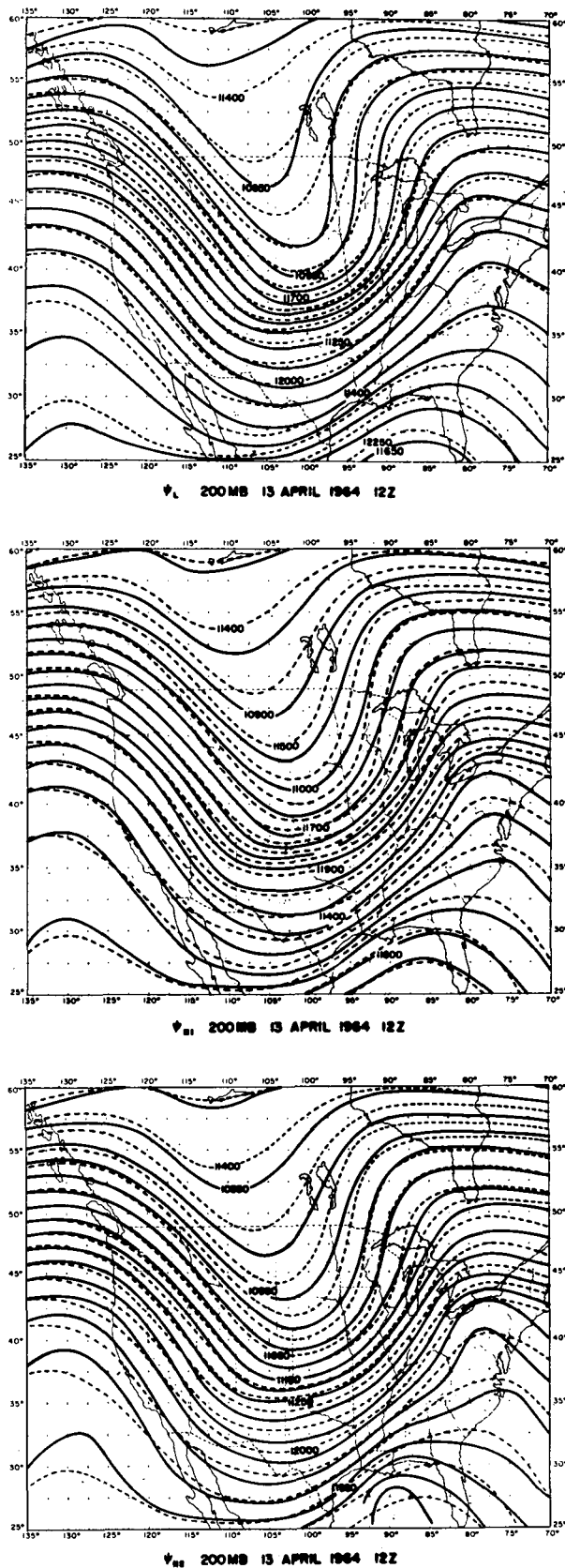


FIGURE 7.—Top: linear balanced stream function, solid lines and geopotential heights of the 200-mb. surface shown as dashed lines. Middle: semi-geostrophic stream function, solid lines and geopotential heights of the 200-mb. surface shown as dashed lines. Bottom: balanced stream function solid lines and geopotential heights of the 200-mb. surface shown as dashed lines.

[1] discussed the nongeostrophic motions downwind from an unstable ridge in the upper flow patterns. One of his findings was that the wind, which is nearly in gradient balance and hence super-geostrophic in the ridges, comes down in a northwesterly flow and cuts towards higher pressure as it acquires a geostrophic adjustment. Such flow fields have been found in the initial states of several of our synoptic investigations of baroclinic frontal cyclone developments. We find that most of this nongeostrophic motion is a nondivergent contribution. And hence it is especially meaningful to compare for instance these four, i) through iv), stream functions listed above.

Figure 7 depicts ψ_L , ψ_{N1} and ψ_{N2} the linear balanced, semi-geostrophic and the complete balanced stream function shown by solid lines in the three drawings. The dashed lines in all these three drawings show the 200-mb. height field during the occlusion state of the wave cyclone. It is not possible to illustrate such drawings for several map times and for several levels, though such information would be very illustrative and pertinent. This depiction of the stream function fields is not quite satisfactory for visual comparisons with the height distributions because the quantities we are most interested in are the speed and directions of the nongeostrophic departures in the non-divergent flow. We have estimated the speeds from these stream functions and the following results were obtained.

Cross isobaric flow is a minimum for the linear balanced stream function ψ_L , the amplitudes of the waves in the westerlies for the z and ψ_L fields are very nearly the same. However, the magnitude of the linear balanced wind is considerably larger near regions of strongly curved flow; in such regions ψ_L overestimates the magnitude of the wind. This effect is especially pronounced in the lower troposphere where closed centers are more in number, typical magnitudes of linear balanced wind are nearly twice as large as the geostrophic or the observed wind. We made some attempts to use the linear balanced stream function to evaluate the divergent part of the wind V_χ and the vertical motion ω from a linear balanced model. The magnitudes of the vorticity and the thermal advection were somewhat too large and unreasonably large rising and sinking motions were found near closed centers. Since the governing equation for the nondivergent stream function is linear this result should become apparent from an analysis of the problem for an analytic distribution of the geopotential height field.

The winds obtained from the semigeostrophic stream function ψ_{N1} and the complete nondivergent stream function ψ_{N2} have speeds very close to the observed or the analyzed wind. The fields of these stream functions are very similar, there is considerable cross-isobaric flow in these two representations. The nondivergent wind cuts towards higher pressure in the northwesterly current and towards lower pressure in the southwesterly flow. The amplitude of the nondivergent stream function is somewhat larger than that of the geopotential heights. This feature may be observed in figure 7 very distinctly in the region south of 40°N. Typical magnitudes of the nongeostrophic departures are as large as 14 m.p.s.

We have also reexamined a case study reported recently by Newton and Palmén [5] on the nongeostrophic winds in a long wave in the westerly current. Similar results were obtained as for the case study we have presented here.

In summarizing it may be stated that a *large part of the upper tropospheric cross-isobaric flow frequently observed in baroclinic disturbances may be explained from the non-divergent part of the total wind.*

4. PARTITIONING OF BAROCLINIC VERTICAL MOTIONS IN THE TWO LEVEL QUASI-GEOSTROPHIC MODEL

We refer here to the simple ω -equation of the quasi-geostrophic dynamics applied to two levels, the 1000- and 500-mb. surfaces.

The baroclinic development of the wave cyclone was well marked with intense centers of sinking and rising motions of air in the middle troposphere. A line was drawn for the four map times through the axis of maximum rising and sinking motions in figure 2 and a partitioning of the vertical motion at the 500-mb. surface was carried out to resolve its two components:

- i) Contribution by differential vorticity advection, ω_1 .
- ii) Contribution by the Laplacian of thermal advection, ω_2 . In general, since cold air is sinking and warm air is rising, the axis in question here marks the line along which a maximum contribution to the release of potential energy takes place for each stage of the storm development.

From earlier synoptic investigations of Petterssen [8] the lee cyclone development is described to follow along the rather well accepted rule: If a region of strong upper positive vorticity advection were found to overlie an open wave cyclone at the sea level, then the wave cyclone will intensify. In terms of the ω -equation Petterssen's rule may be reexpressed as follows: In the initial stages of a cyclone development differential vorticity advection is important and in later stages as the cyclone advects warm and cold air by its circulation, Laplacian of thermal advection would increase. This has been an accepted rule of synoptic meteorologists for a considerable time. This rule is also in accordance with a principle generally used in current weather map discussions regarding the intensification of a diffluent upper trough and the associated surface cyclone development (see figs. 1 and 2). Here again the synoptic rules are that the initial intensification processes are quasi-barotropic and the baroclinic processes, namely the thermal effects, became important only somewhat later.

The proposed partitioning of the vertical motions during the various stages of the storm development will be very important in verifying the validity of these synoptic principles quantitatively. Figure 8a shows the partitioning at the diffluent trough stage. The solid line indicates the total vertical motions, the dashed line the thermal term, and the dash-dotted line the differential vorticity advection term. During this stage air is sinking behind the upper diffluent trough strongest sinking motion $\approx 550 \times 10^{-5}$

mb./sec. which corresponds to about 8 cm./sec. at the 500-mb. surface. The rising motion ahead of the trough is very weak and of the order 1 cm./sec. The interesting aspect of the partitioning at this stage is that both the thermal term (cold air advection) and the vorticity advection give about equal contribution at this time. Hence we must conclude that at the initial diffluence stage both the vorticity and the thermal mechanisms are operating with about equal intensity, the latter by no means is negligible. This conclusion could have been drawn from an examination of the isothermal patterns below the upper trough which reveal a lag of the thermal trough with respect to the pressure trough and attendant large cold advection. An examination of figures 8b, c, and d show the gradual increase of the sinking and rising motions along the line under investigation. During the open wave stage, figure 8b, both terms contribute about equally in the rising air whose intensity has increased to about 5.5 cm./sec., in the sinking branch the thermal contribution is somewhat larger. There is an interesting phase lag between the two terms (represented in this manner) and there are regions in the vicinity of the trough where the two effects cancel. During the pre-occlusion stage the storm has a larger baroclinic effect evidenced by the much larger magnitudes of the thermal term. At the occlusion stage sinking motions acquire intensities near 13 cm./sec. and rising motions near 11 cm./sec. The sinking motion is mostly a thermal contribution, weak sinking motions about 10 percent are contributed by the differential vorticity advection. Ahead of the trough most of the rising motion, about 65 percent, is contributed again by warm air advection. At this stage the thermal trough was somewhat ahead of the upper pressure trough. This is substantiated by the latitude of the zero vertical motion in the two terms.

Figure 9 shows the distribution maps of ω , ω_1 , and ω_2 for the final map time and one may observe the relative importance of the baroclinic mechanisms. The total rising motion is largely a thermal contribution over most of the map. This implies that $J(T, \nabla^2 z) \approx -J(z, \nabla^2 T)$ when the baroclinic disturbance is most intense; the advection of vorticity by the thermal wind is nearly equal and opposite to the advection of thermal vorticity by the geostrophic wind. This is not quite true in the vicinity of the upper trough where the vorticity contribution is somewhat large. This study has been repeated for seven examples of extratropical storms, in none of which the contribution by thermal advection was small initially. All of these storms were studied over continental United States.

5. RESULTS OF PARTITIONING OF VERTICAL MOTIONS FROM THE MULTILEVEL BALANCE MODEL

DIFFERENTIAL VORTICITY ADVECTION

A map of corresponding vertical motion is displayed in figure 10 (top); only the last map time is included in the list of illustrations. Vertical motions are somewhat cellular but the major features include rising air ahead of the upper trough and sinking behind. There is a considerable separa-

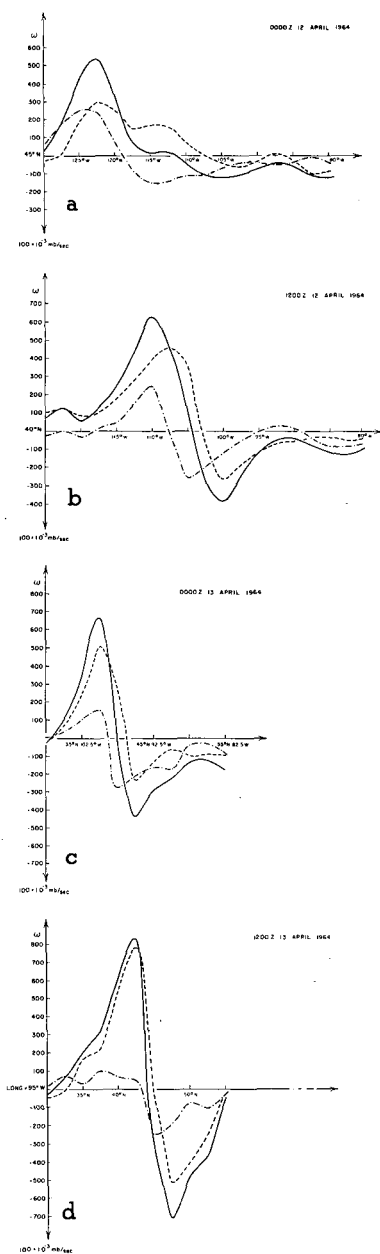


FIGURE 8.—Partitioning of quasi-geostrophic vertical velocity along a line connecting maximum rising and sinking motions, for four map times: a) 0000 GMT, April 12, 1964; b) 1200 GMT, April 12, 1964; c) 0000 GMT, April 13, 1964; and d) 1200 GMT, April 13, 1964. Solid line: total contribution. Dash line: thermal contribution. Dash-dot line: vorticity contribution.

tion between the regions of largest upward and downward vertical motions. Largest rising motions are of the order -500×10^{-5} mb./sec. over Minnesota, north of the surface Low. This corresponds to about 7 cm./sec. The intensity of the largest sinking motions is in the lee of the Rockies and is of the same intensity. This pattern of rising motion contribution is not quite similar to the contribution by differential vorticity advection in a 2-level quasi-geostrophic model (fig. 9, bottom right). These differences can arise due to at least four reasons.

- i) Static stability is variable in the balance model.
- ii) Differential advectations take into account the strong jet stream at the 300-mb. surface in the balance model.

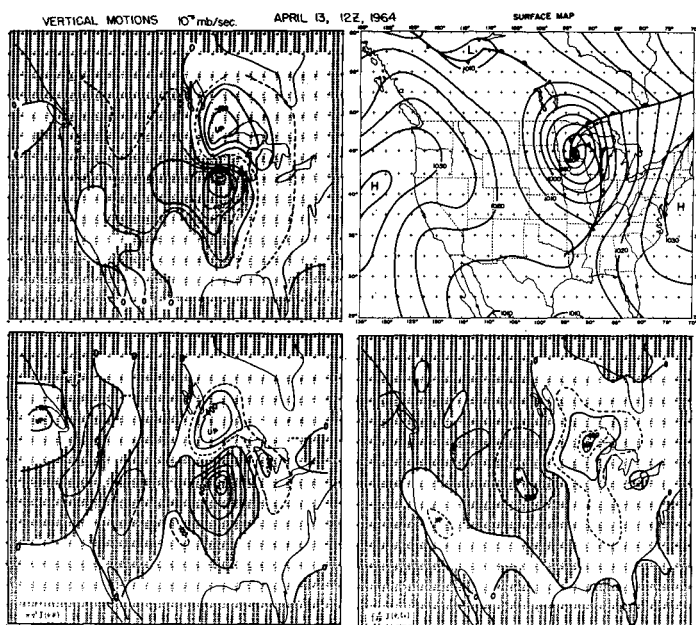


FIGURE 9.—Top left: total quasi-geostrophic vertical velocity from a 2-level model, at the 500-mb. surface. Top right: surface isobars. Bottom left: quasi-geostrophic vertical velocity from a 2-level model, at the 500-mb. surface. (Thermal contribution.) Bottom right: quasi-geostrophic vertical velocity from a 2-level model, at the 500-mb. surface. (Vorticity contribution.)

iii) Balance stream function ψ_N is different from the geostrophic stream function, gz/f_0 .

iv) Coriolis parameter f is variable in the balance model. Of these iii) and iv) cannot account for the large differences in the two models, especially magnitudes of the order of 300×10^{-5} mb./sec. in the lee of the Rockies. It cannot be explained in terms of the variable static stability because in the cold air σ is larger in the balance model hence ω would tend to become smaller by this effect. The product of σ times ω is approximately invariant in these models. The large difference is best explained by ii), namely better vertical resolution in the multilevel balance model. These large differences are found in the region of the strong jet stream; the differential vorticity advection of the balance model does take these features into account.

LAPLACIAN OF THERMAL ADVECTION

The thermal contribution to rising and sinking motion is large (fig. 10, bottom); as we shall see from the remaining terms, it is the dominant term. Sinking motion in the cold air behind the surface front acquires magnitudes close to 1200×10^{-5} mb./sec. downward motion at the 500-mb. surface. This field is somewhat different from the corresponding quasi-geostrophic contribution (fig. 9, bottom left). The balance wind, used for advection of the thermal field, is closer to the gradient and the actual wind which is subgeostrophic near low centers. The large differences near the low center cannot be explained by this difference in the stream functions. Part of this difference is still due to the stream functions used in the two calculations. In the quasi-geostrophic calculation the stream function refers to 750-mb. surface, while for the multilevel balance model it corresponds to the 500-mb. surface. Another



FIGURE 10.—Top: contribution to balance vertical motion—differential vorticity advection. Bottom: contribution to balance vertical motion—Laplacian of thermal advection.

reason for the difference is the intensity of cold advection which was stronger at the upper levels.

DEFORMATION AND DIVERGENCE CONTRIBUTIONS

The contribution to the vertical velocity by the deformation and divergence effects (fig. 11) are somewhat similar near the low center. They both counteract the rising and sinking contributions produced by the two leading terms. The large rising center, southwest of Lake Michigan has an intensity close to -300 units, which is approximately 4 cm./sec. rising motion at the 500 -mb. surface. It is thus clear that these terms are very important in the storm dynamics. The deformation term is generally very small away from the storm, but there are several centers >100 units in the divergence contribution. In general the divergence contribution counteracts the contribution by the two leading terms (fig. 10) over most regions. Both of these terms do not appear in the quasi-geostrophic theory, and hence these results are quite significant.

FRICTIONAL AND TERRAIN CONTRIBUTIONS

Drag coefficient C_D is equal to 2.5×10^{-3} , in this study. Largest frictional vertical motion (fig. 12) are of the

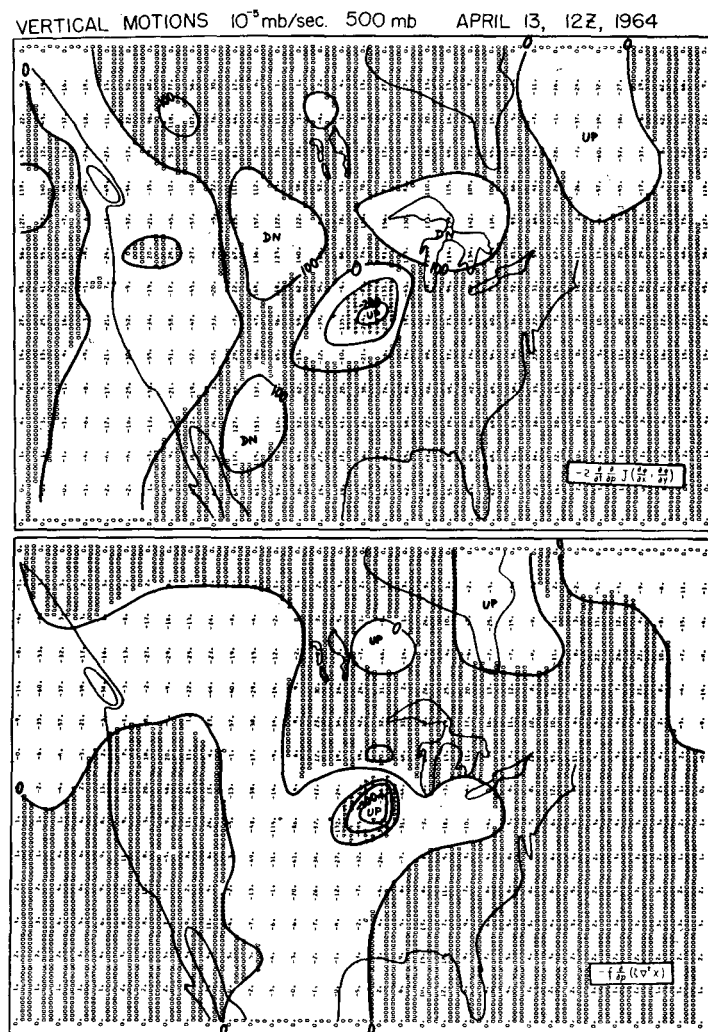


FIGURE 11.—Contributions to balance vertical motion. Top: deformation term. Bottom: divergence term.

order 10^{-3} mb./sec. at the 900 mb.

In regions of cyclonic low level relative vorticity rising motion is well organized, and in regions of anti-cyclonic vorticity sinking motion is found. This is to be expected for this simple formulation of the frictional stress terms. Figure 12 (bottom) shows the horizontal distribution of the frictional contribution, shown by solid lines, and the surface pressure field (± 5 -mb. isobars) are indicated by dashed lines. Both terrain and the frictional contribution decay rapidly with height. Figure 13 shows an example of the vertical distribution of the damping of the frictional vertical velocity taken at a grid point. Whether indeed such frictional vertical velocities exist over land areas can not be checked very easily, it is however comforting to note that the total picture of the mid-tropospheric vertical velocity is not altered by more than 10 percent when frictional and terrain effects are introduced. Danielsen [2] has compared the magnitudes of midtropospheric vertical motion obtained from isentropic trajectory calculation and those obtained from solutions of our balanced model (without terrain and friction) and found very good agreement. It leads us to conclude that the effect of friction and terrain should be very small ($\ll 10^{-3}$ mb./sec.) in the middle troposphere

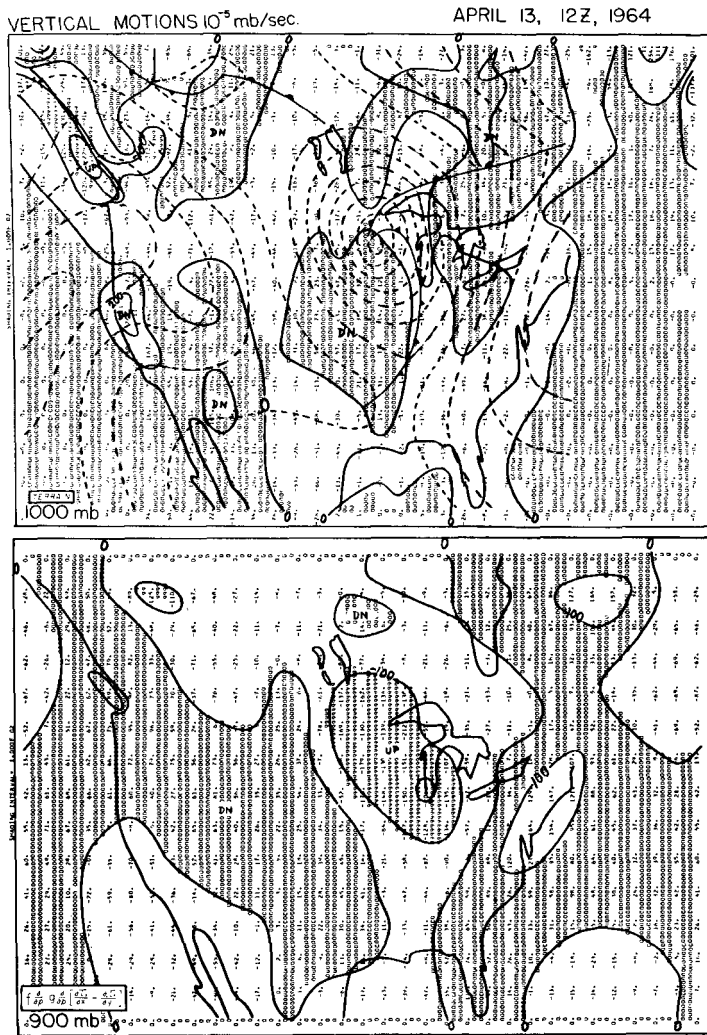


FIGURE 12.—Top: contribution to balance vertical motion at 1000-mb. surface terrain effect. The dash lines indicate the surface isobars. Bottom: contribution to balance vertical motion by surface frictional stresses at the 900-mb. surface.

and hence the formulation presented here is perhaps not very unrealistic. The corresponding contribution at other map times were quite similar. Terrain effects were larger at the first map time behind the upper trough and contributed significantly to the total sinking motion and the associated lee development.

CONTRIBUTION BY RELEASE OF LATENT HEAT

Partitioning of latent heat contribution is carried out by setting,

$$\nabla^2 \sigma \omega_L + f^2 \frac{\partial^2 \omega_L}{\partial p^2} = \frac{RL}{c_p p} \nabla^2 \omega \frac{\partial q_s}{\partial p}$$

ω_L is the contribution by latent heat and ω is the vertical velocity obtained by solving the complete balance equations. We may write,

$$\omega = \omega_L + \omega_R$$

where ω_R is the contribution by the remaining terms. We may rewrite the ω -equation of this problem in the form,

$$\nabla^2 \sigma_e \omega_L + f^2 \frac{\partial^2 \omega_L}{\partial p^2} = \frac{RL}{c_p p} \nabla^2 \omega_R \frac{\partial q_s}{\partial p}$$

This equation will be elliptic if $\sigma_e > 0$. Calculations are

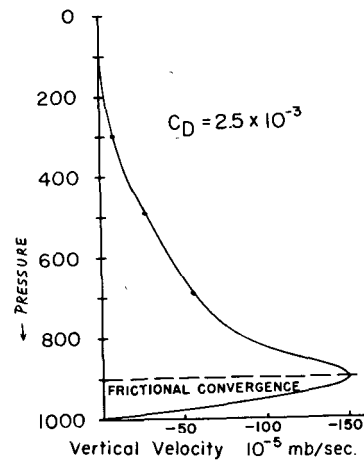


FIGURE 13.—Decay of frictional vertical velocity plotted against pressure (ordinate) for a selected point from figure 12 (bottom).

made assuming no conditionally unstable regions. This requires an adjustment of the effective static stability,

$$\sigma_e = \sigma - \frac{RL}{c_p p} \frac{\partial q_s}{\partial p}$$

In regions, where $\sigma_e < 0$ we have arbitrarily set $\sigma_e = 0.1\sigma$. this artificial setting was carried out at few grid points south of 30°N. near the Gulf of Mexico in the moist and warm tongue of air. As we have mentioned earlier this is the region where a special form of heating function should have been evaluated in terms of parameterization of cumulus scale motion. We hope to present such results in the near future.

Figure 14 shows the contribution to the vertical velocity from latent heat at the 900-, 700-, 500-, and 300-mb. surfaces. The results show that the latent heat contribution is very large, >500 units, and comparable to the first two. The corresponding contribution at the first three map times was much smaller. The rising motion center gradually moves eastward (fig. 6), while the moisture field is quasi-stationary. The significance of these vertical motions to the intensification of the surface pressure field during the last 12 hr. becomes clearer from this analysis. The magnitude of low level convergence and the product of absolute vorticity and convergence is large in the vicinity of the intensifying Low. The patterns of rising motion (fig. 14) show that even at 300-mb. surface latent heat contributions are of the order -50×10^{-5} mb./sec. This corresponds to about 1 cm./sec. rising motion. Another feature of the ω -equation, not quite understood here, is the sinking motion distribution that spreads out away from regions of heating. It is not obvious whether the real atmosphere indeed has this feature. The intensity of the sinking motion is quite small. This numerical feature is found in both high and low latitude investigations where the nature of the heating terms are quite different.

AN OVERALL LOOK AT ALL THE TERMS

Table 1 shows a distribution of vertical motion at the 500-mb. surface along a line taken parallel to the upper

trough and 5° long. east or downward from the trough. Different points from left to right on table 1 are taken from south to north. They may be identified easily from the figures of individual charts presented earlier.

Partitioning shows the following features of interest. Ahead of the upper trough vorticity advection (1) contributes rising motion at all points; to the south cold air advection (2) produces sinking motion while to the north the first two terms are in phase. This is a very typical feature of the thermal and vorticity contribution in the near occlusion stage in extratropical storm. Ahead of the trough contribution by the deformations term (3) is large and cuts down the intensity of rising motion. The divergence term (4) counteracts the rising and sinking motion of the total picture; its contributions along this line are not as strong as they are usually found behind intense cold fronts. Frictional contribution (5) above the Low is rising motion, intensity about 6/10 cm./sec. The contribution by latent heat (6), very large north of the surface Low, shows a large point value, a feature typical of heating distribution. Lake water temperatures were analyzed to examine their contribution to development through sensible heat transfer (7); this was a very small effect in this storm and is almost negligible at the 500-mb. surface. The vertical motions from vertical advection (8) and the twisting terms (9) are small; the latter is in phase with the vorticity advection (1) contribution while the former is out of phase. The two contributions (8) and (9) have a tendency to cancel each other. The contributions by the vorticity (10) and thermal (11) advection by the divergent part of the wind are both very small over all regions. The beta term (12) is the smallest of all of the contributions and contributes less than 1/10 cm./sec. rising or sinking motion. The partitioning was done without terrain effects. A comparison of the total without terrain effects (sum of partitioned ω) and the solution of the complete problem with the terrain is shown in the last two rows of table 1. Terrain contribution damp with height

rapidly, hence the totals in the last two rows (at 500-mb. surface) are nearly identical.

Table 1 and the charts presented earlier give an insight into the processes and important mechanisms in the middle troposphere. We have only displayed a small part of information. Many such charts are available at several levels of the troposphere where the ratio of the relative magnitudes are not the same as what we have portrayed in table 1.

Figure 15 shows a distribution of the vertical velocity, ω , at the 500-mb. surface from the complete balance model including the 12 internal forcing functions and one external (terrain) boundary forcing function. There are four results of importance that may be compared at this stage: (Apr. 13, 1964, 12 GMT)

- i) Two level quasi-geostrophic ω , figure 9 (top left)
- ii) Multilevel linear balance ω , figure 6 (bottom right)
- iii) Multilevel balance ω containing sum of two leading terms, figure 15 (bottom)
- and
- iv) Multilevel balance ω containing sum of all terms, figure 15 (top).

It is of interest to note that the patterns of total vertical velocity are similar in all cases; the intensities are somewhat different. Inclusion of latent heat increases the rising motion; and the deformation and divergence effects cut down the intensity of sinking motion in the complete model.

6. ON THE DEVELOPMENT OF THE APRIL STORM

Analysis of the forcing functions of the ω -equation, their individual contribution to rising motion, and an examina-

TABLE 1.—Contribution to the vertical motion by different forcing functions

Forcing functions	Vertical motion in units 10 ⁻⁵ mb./sec. at different points							
	1	2	3	4	5	6	7	8
1. $f \frac{\partial}{\partial p} J(\psi, \zeta a)$	-121	-135	-14	-63	-326	-266	-255	-171
2. $\pi \nabla^2 J(\psi, \theta)$	35	128	180	82	-37	-257	-258	-7
3. $-2 \frac{\partial}{\partial x} \frac{\partial}{\partial p} J \left(\frac{\partial \psi}{\partial x} \frac{\partial \psi}{\partial y} \right)$	88	74	18	-43	173	130	82	9
4. $-f \frac{\partial}{\partial p} (\zeta \nabla^2 \chi)$	6	-7	-31	-44	48	31	2	-14
5. $f \frac{\partial}{\partial p} \theta \frac{\partial}{\partial p} \left[\frac{\partial r_y}{\partial x} \frac{\partial r_x}{\partial y} \right]$	-8	-14	-19	-47	-41	-38	-32	-17
6. $-\frac{R}{c_p D} \nabla^2 H_L$	1	6	7	14	-14	-13	-372	-27
7. $-\frac{R}{c_p D} \nabla^2 H_S$	0	0	0	0	1	1	1	1
8. $f \frac{\partial}{\partial p} \left(\omega \frac{\partial}{\partial p} \nabla^2 \psi \right)$	13	15	10	15	13	16	78	35
9. $f \frac{\partial}{\partial p} \left(\nabla \omega \cdot \nabla \frac{\partial \psi}{\partial p} \right)$	-14	-23	-21	-26	-19	-10	-8	-18
10. $-f \frac{\partial}{\partial p} (\nabla \chi \cdot \nabla \zeta a)$	9	26	25	29	38	15	-9	0
11. $-\pi \nabla^2 (\nabla \chi \cdot \nabla \theta)$	-6	-7	-15	8	22	29	18	2
12. $-\beta \frac{\partial}{\partial p} \frac{\partial}{\partial y} \frac{\partial \psi}{\partial x}$	10	7	2	-5	-7	-8	-7	-4
Total without terrain	13	70	141	-80	-151	-370	-761	-212
Total with terrain	13	71	141	-79	-150	-370	-761	-212

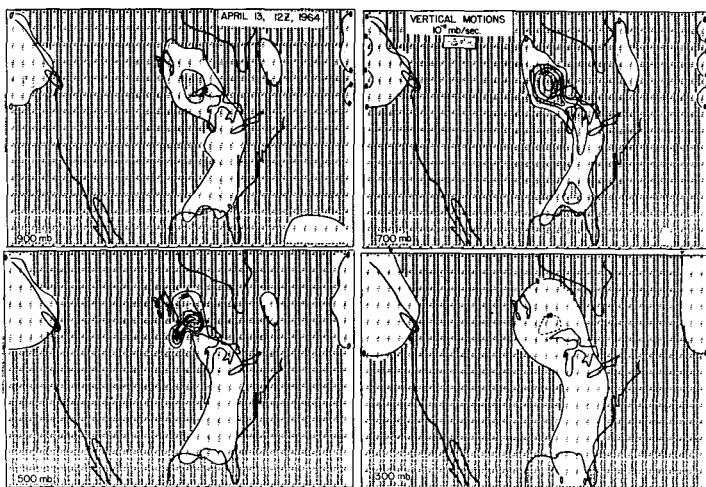


FIGURE 14.—Contribution to the balance vertical motion from latent heat release at the 900-, 700-, 500-, and the 300-mb. surface. Pressure levels and magnitudes are indicated on the maps. (April 13, 1964, 12 GMT.)

tion of the distribution of different terms of the vorticity equations enables us to draw the following description of the storm development.

The initial development April 12, 00 GMT–April 12, 12 GMT was at upper levels behind the diffluent trough. Strong sinking motions are produced by differential vorticity advection, Laplacian of thermal advection, and the terrain effects. Above the level of nondivergence (near 500 mb.) in this sinking region a strong field of horizontal convergence exists. Parcels moving southeastward experience a strong production of absolute vorticity in this region. The development at upper levels results in a drop of surface pressure field ahead of the upper trough.

The final surface development between April 13, 00 GMT–12 GMT is contributed by differential vorticity advection, Laplacian of thermal advection, latent heat, and surface friction. Parcels moving through the lower levels experience strong convergence in the rising motion produced by these effects. The product of $\partial\omega/\partial p$ and ζ_a is indeed very large and these factors contribute significantly. The divergence and deformation effects counteract the development and have a significant effect on the storm dynamics. Some of the other forcing functions that appear to be small in the instantaneous picture may have contributed significantly over longer time scales. Such questions can only be answered by examining a prediction approach to this problem.

Paegle [6] has computed three dimensional trajectories from the ψ , χ , and ω fields of a balance model, and has discussed some aspects of the development problem; this study presents quantitative measures of the development terms along the trajectories.

ACKNOWLEDGMENTS

Principal financial support for the work described in this paper was obtained from Air Force Cambridge Research Laboratory, Bedford, Mass., during the period November 1964–November 1966. Dr. Carl Krietzberg of AFCRL and Professor Edwin Danielsen of Pennsylvania State University provided considerable encouragement for the continuation of this work.

Partial financial support was also received from ESSA grant number: E 65-67 (G) through Dr. Fred Shuman, National Meteorological Center, and from NASA grant number: NsG 237-62 through Professor Gordon MacDonald, Institute of Geophysics at UCLA.

Mr. John M. Brown, now a graduate student at MIT, was a part of many of our discussions. Mr. Robert M. Coie, a senior programmer for IBM at Douglas Aircraft Company at Long Beach, Calif., was a consultant on some of the coding aspects. He provided considerable clarification and efficiency.

Computations were performed on the IBM 7094 computer; we are grateful to the Computing Facility of UCLA for their generous support.

REFERENCES

1. J. A. B. Bjerknes, "Extratropical Cyclones," *Compendium of Meteorology*, American Meteorological Society, Boston, 1951, pp. 577–598.
2. E. F. Danielsen, "Research in Four-Dimensional Diagnosis of Cyclonic Storm Cloud Systems," *Scientific Report No. 1*, Contract AF(628)-4762 AFCRL-66-30, Pennsylvania State University, University Park, 1966, 53 pp.

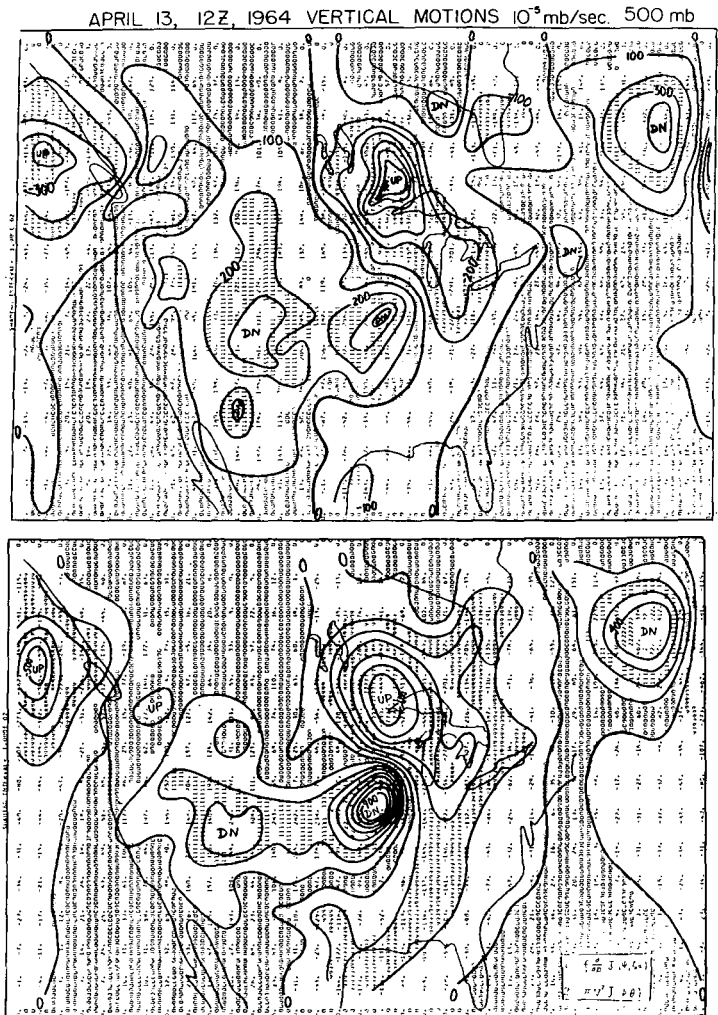


FIGURE 15.—Top: total balance vertical motion including contributions of 12 forcing functions and terrain. Bottom: balance vertical motions, sum of contribution from differential vorticity advection and Laplacian of thermal advection.

3. T. N. Krishnamurti, "A Diagnostic Balance Model for Studies of Weather Systems of Low and High Latitudes, Rossby Number less than 1," *Monthly Weather Review*, vol. 96, No. 4, Apr. 1968, pp. 197–207.
4. T. N. Krishnamurti, J. Nogués, and D. Baumhefner, "On the Partitioning of the Baroclinic Vertical Motions in a Developing Wave Cyclone," *Scientific Report No. 1*, Contract AF 19(628)-4777 AFCRL-66-419, Dept. of Meteorology, University of California at Los Angeles, 1966, 33 pp.
5. C. W. Newton and E. Palmén, "Kinematic and Thermal Properties of a Large-Amplitude Wave in the Westerlies," *Tellus*, vol. 15, No. 2, May 1963, pp. 99–119.
6. J. Paegle, "Numerical Calculation of Three Dimensional Trajectories Utilizing the Balanced Horizontal and Vertical Motions," Final Report, *Diagnostic Studies of Weather Systems of Low and High Latitudes (Rossby Number < 1)*, Contract AF 19(628)-4777, AFCRL-67-0128, Dept. of Meteorology, University of California at Los Angeles, Apr. 1967, pp. 1–21.
7. S. Petterssen, "Contribution to the Theory of Frontogenesis," *Geofysike Publikasjoner*, Oslo, vol. 11, No. 6, 1936, 27 pp.
8. S. Petterssen, *Weather Analysis and Forecasting*, The McGraw-Hill Book Co., Inc., New York, vol. 1, 2d Edition, 1956, 428 pp. (see Chapter 16, pp. 320–338).
9. N. A. Phillips, "Geostrophic Motion," *Reviews of Geophysics*, Washington, D.C., vol. 1, No. 2, May 1963, pp. 123–176.